Spatiotemporal investigation of visible radiation distribution around attachment-detachment transition on Wendelstein 7-X

G. Cseh[1], A. Buzas.[1], M. Jakubowski[2], G. Kocsis[1], M. Kriete[3], V. Perseo[2], T. Szepesi[1], D. Zhang[2] and the W7-X Team[1]

[1] *HUN-REN Centre for Energy Research, Institute for Atomic Energy Research, Konkoly-Thege út 29-33, 1121 Budapest, Hungary*
[2] *Max-Planck -Institut für Plasmaphysik, D-17491 Greifswald, Germany*
[3] *Auburn University, Alabama, USA*

Detachment is an active and important research topic of magnetically confined fusion experiments. During detachment, a significant fraction of thermal power is dissipated as radiation, which reduces heat and particle load on the divertor target plates. This makes it a promising candidate for an exhaust solution in future fusion power plants. On Wendelstein 7-X (W7-X) detachment is routinely achieved, a stable detachment lasted for 110 s was already demonstrated, during which the heat flux to the divertor target plates was negligible [1].

Understanding the changes in the transport processes around the attachment-detachment transition is of utmost importance not just in terms of getting a deeper insight into the process itself, but also to further optimize the operational scenarios.

The Event Detection Intelligent CAMera (EDICAM) overview camera system [2] can observe the majority of the plasma volume of W7-X. The EDICAMs has a view at the inner wall, where – after a spatial calibration and in the presence of plasma – the observed radiation patterns can be localized, since they are at the plasma edge and relatively cool to produce radiation in the visible range. Using this view and visualizing the magnetic field lines following the X- and O-points, the dynamics of the radiation distribution around these points can be observed in time.

During detachment the divertor radiation is getting less intense than in the attached phase. Usually, field-aligned structures brighten up around some of the X-points and inside some islands, especially at the inboard side of the device. The purpose of this contribution is to develop a method to derive these radiation distributions and compare the detachment dynamics for different cases.

The EDICAM compact fast cameras are sensitive in the visible range (used without any filter). They can resist the magnetic field (<3 T). These two properties make them ideal for using in fusion experiments, where they can be placed in the vicinity of the plasma. The system consists of 10 EDICAM cameras, which are routinely running with a 100 FPS recording rate and looking at a tangential view of the torus interior (see Fig. 1).

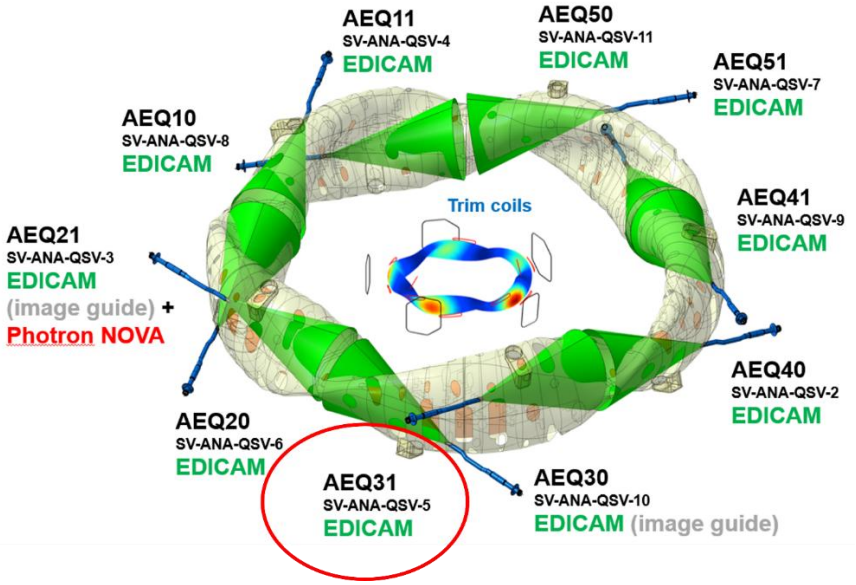

Fig. 1. The EDICAM overview system. The EDICAM looking at W7-X port AEQ31, which is used for the present investigation is circled with red on the figure.

Using their view a region-of-interest (ROI) can be defined at the edge of the machine, where they can detect localized, visible radiation. In the present work, the camera looking from the AEQ31 port is used (see red circle in Fig. 1). The spatial calibration of the cameras is done by Calcam [3] using the W7-X CAD model.

The ROI defined for this investigation can be seen on Fig. 2. Using the O_1, X_1 and O_2 points and their corresponding field lines as a starting point, new lines are interpolated between them. This way, we get a "vertical" resolution between the X- and O-points. The full ROI defined the above-described way is marked with purple on Fig. 2. After the definition, the pixel intensities were sampled along those lines and were averaged. This way, for every image in an EDICAM recording, a "vertical" average intensity distribution is created, which contains two O-points and one X-point. Using all of these distributions for all images in a given EDICAM recording, the radiation dynamics can be observed. Looking at detachment experiments, the attachment-detachment transition dynamics in terms of the visible radiation distribution change and the movement of the field-aligned structures can be investigated.

For the present contribution, two experiments were chosen from the last campaign of W7-X. 20250313.028 is an experiment with a standard magnetic configuration, but in reversed field (EIM000-2620). In this experiment, density steps were taken (one at 9 s and one at 12 s, see Fig. 3). Corresponding to this, the radiation power (P_{rad}) is also increased. The heating power was the same for the whole experiment. The other experiment is almost identical to the previous one, except that it has been done with forward field configuration (EIM000+2614) and four density steps were taken (at 3 s, 6 s, 9 s and 12 s). The radiation power also increased at the density steps, but at 9 and 12 s it was rather like an oscillation based on the P_{rad} signal.

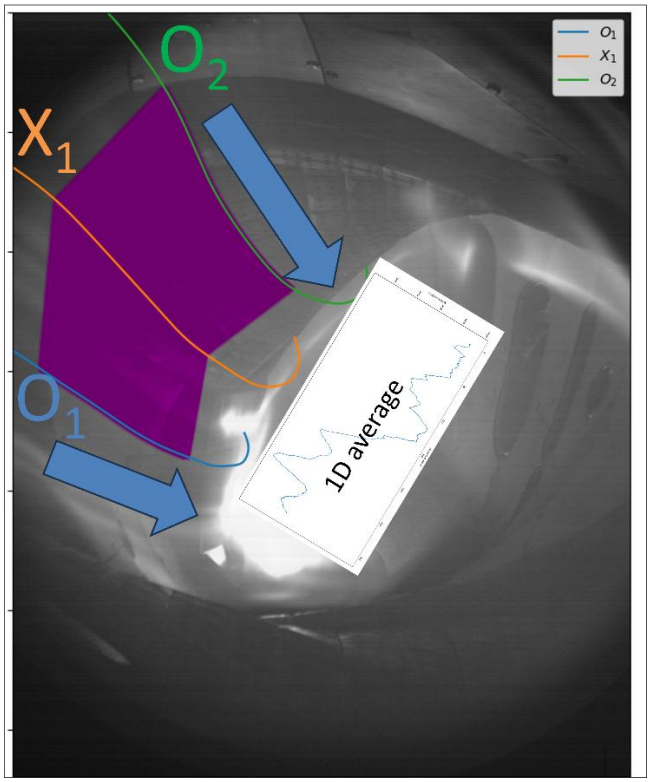

Fig. 2. ROI definition and scheme of the method. O_1, X_1 and O_2 points and their corresponding field lines were used along with interpolated lines between them to produce a 2D ROI. The sampled pixel intensities were averaged along these lines and a "vertical" 1D average pixel intensity distribution is generated per image.

Using the above-described method and the two experiments, the 2D image was created for both experiments. Several interesting properties can be found.

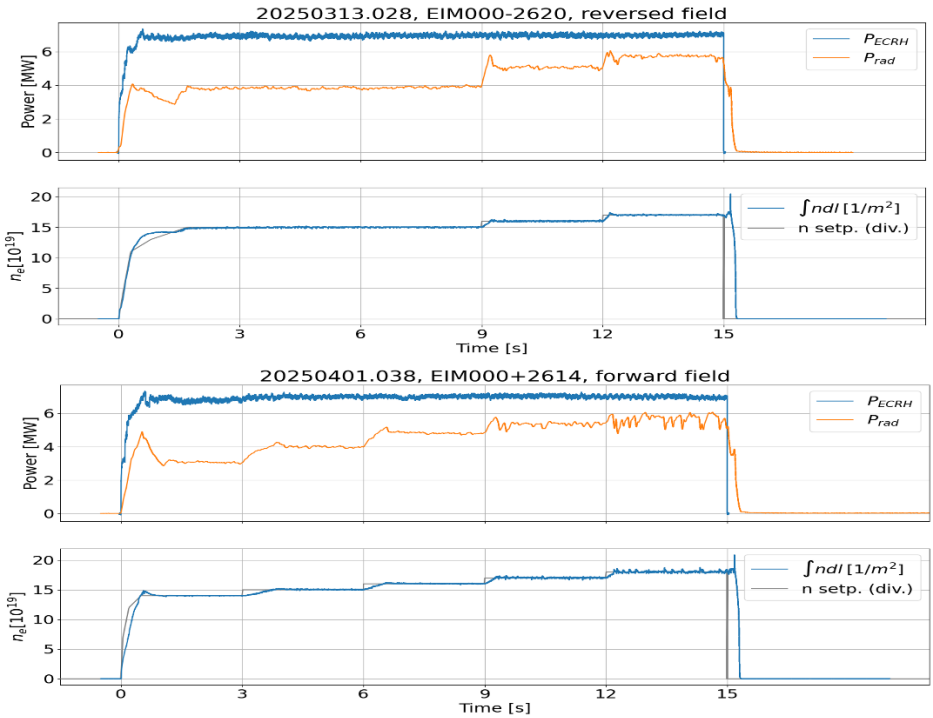

Fig. 3. Experiments chosen for the present investigation. Top: 20250313.028, standard configuration, reversed field. Bottom: 20250401.038, standard configuration, forward field. For both experiments, ECRH heating power, radiation power, and the line integrated density is shown.

First of all, looking at the upper part of Fig. 4 (standard magnetic configuration, reversed field), it can be seen that at the beginning, no prominent field-aligned structures can be observed. The first such structures appear at around 1.5 s. This situation does not change until

9 s, where the first density step is taken and the radiation fraction ($f_{rad} = P_{ECRH} / P_{rad}$) is going up to 0.75. At this point, the prominent field-aligned structure between $O_1 – X_1$ and $X_1 – O_2$ gets brighter (this is presumably the part which interacts with the divertor), but also another structure is getting more pronounced near the X-point. This is getting even closer to the X-point at 12 s, the next density step, where f_{rad} is going up to 0.8.

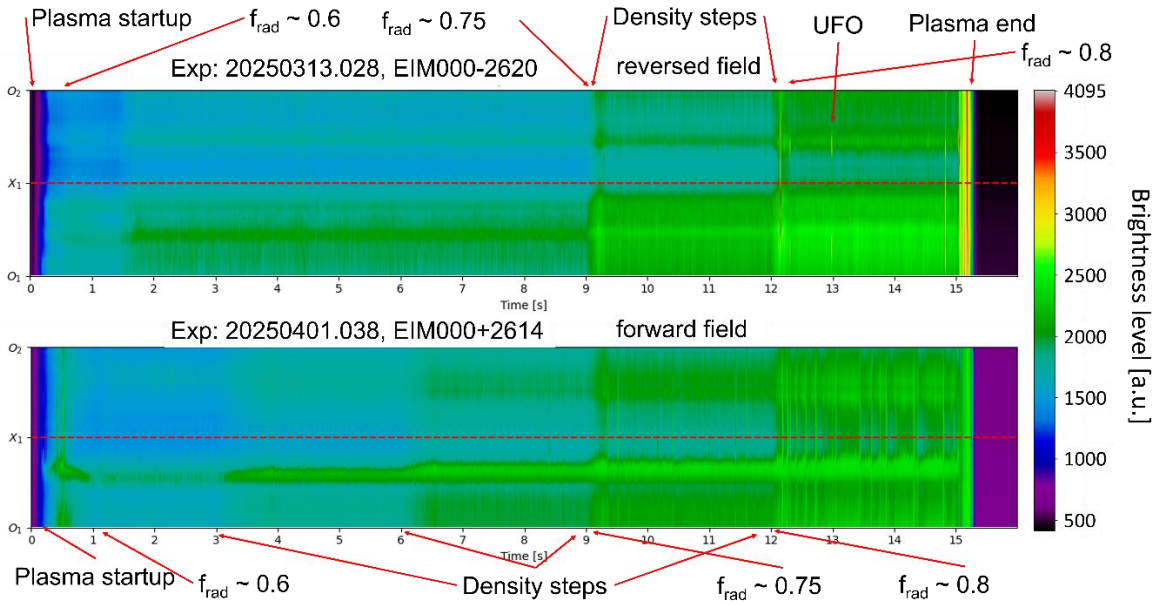

Fig. 4. Detachment dynamics in the visible range for the two experiments shown in Fig. 3.

This suggests that **the radiation zone shifts toward X_1 as f_{rad} increases**. The region between O_1 and X_1 is generally brighter than the region between X_1 and O_2. This could be a property of the camera view but needs further investigation.

Looking at the lower part of Fig. 4 it can be observed that it is similar to the upper part, but the second field-aligned structure does not appear close to the X-point, but the whole field-aligned structure region is getting wider towards the X-point. All density steps can be identified and the oscillational nature of the P_{rad} signal at the end of the experiment can be observed as well (see the lower part of Fig. 3). In the future, more cameras and more configurations will be compared.

Acknowledgement: This work has been carried out within the framework of the EUROfusion Consortium, funded by the European Union via the Euratom Research and Training Programme (Grant Agreement No 101052200 - EUROfusion). Views and opinions expressed are however those of the author(s) only and do not necessarily reflect those of the European Union or the European Commission. Neither the European Union nor the European Commission can be held responsible for them.

References

[1] Grulke, O., C. Albert, JA Alcuson Belloso, P. Aleynikov, K. Aleynikova, A. Alonso, G. Anda et al. "Overview of the first Wendelstein 7-X long pulse campaign with fully water-cooled plasma facing components." *Nuclear Fusion* 64, no. 11 (2024): 112002.

[2] G. Kocsis,.et al. (2015). Overview video diagnostics for the W7-X stellarator. *Fusion Engineering and Design*, *96*, 808-811.

[3] S. Silburn, J. Harrison, M. Smithies, A. Wynn, T. Farley, and J. Cavalier (2018), “Calcam,” Zenodo, version 1.9.4, https://doi.org/10.5281/zenodo.1478555